Korea-Australia Rheology Journal
Vol. 19, No. 3, November 2007 pp. 147-156

Orientation and deformation of FENE dumbbells in confined microchannel and contraction flow geometry

Sunjin Song, Ju Min Kim, Kyung Hyun Ahn*, Seung Jong Lee and Jong-Kee Yeo[1]
School of Chemical and Biological Engineering, Seoul National University, Seoul 151-744, Korea
[1]LG Chemical Limited, Daejon 305-380, Korea

(Received July 9, 2007; final revision received October 7, 2007)

Abstract

The orientation and deformation of polymer chains in a confined channel flow has been investigated. The polymer chain was modeled as a Finitely Extensible Nonlinear Elastic (FENE) dumbbell. The Brownian configuration field method was extended to take the interaction between the flow and local chain dynamics into account. Drag and Brownian forces were treated as anisotropic in order to reflect the influence of the wall in the confined flow. Both Poiseuille flow and 4 : 1 contraction flow were considered. Of particular interest was molecular tumbling of polymer chains near the wall. It was strongly influenced by anisotropic drag and high shear close to the wall. We discussed the mechanism of this particular behavior in terms of the governing forces. The dumbbell configuration was determined not only by the wall interaction but also by the flow type of the geometric origin. The effect of extensional flow on dumbbell configuration was also discussed by comparing with the Poiseuille flow.

Keywords : FENE dumbbell, anisotropic drag, Brownian configuration field, molecular tumbling, wall interaction

1. Introduction

In order to develop and control microfluidic devices in which polymers are flowing as in DNA chips, it is important to understand the dynamics of polymers in the microchannel flow. There are many researches on rheology and configuration of dilute polymer solutions in both shear (Hoagland and Prud'home, 1988; Lee *et al.*, 1997; Smith *et al.*, 1999) and extensional flows (Perkins *et al.*, 1997; Smith and Chu, 1998). They have tried to understand the characteristics of the complex flow and its physical origin. Molecular orientation and deformation of polymers are relatively well known for diverse flow conditions and polymer characteristics (Hoagland and Prud'home, 1988; Lee *et al.*, 1997).

But in the confined flow as in the microfluidic devices, the polymer solution shows an anomalous dynamics and the chain dynamics is quite different from the case in the free shear flow (Doyle *et al.*, 2000; Shrewsbury *et al.*, 2001). Many researches tried to describe the effect of wall on the polymer behavior, focusing on the hydrodynamic interaction and excluded volume effect using repulsive potentials between the wall and polymers. Jendrejack *et al.* (2003a; 2003b) showed DNA migration and the configurational change due to confinement by considering the hydrodynamic interaction at the wall. Skjetne *et al.* (1997) showed the bending and curvature of fibers caused by the wall interaction and hydrodynamic interaction in the simple shear flow, leading quite different rheology and configurations near the wall. Radzyner and Rapaport (1998) simulated flexible and rigid molecules, and described the orientational effect using molecular dynamics (MD) simulation in Poiseuille flow. In their work, there was a competition between the Maxwell orientation in which the molecule tends to align at 45° to the flow direction and a tendency of molecules close to the wall to align parallel to the flow direction. Woo *et al.* (2004a) pointed out that as a consequence of chain confinement, the entropic force is altered by the loss of chain configurational space, and the viscous drag on the chain is increased due to the hydrodynamic interaction with the wall. They also reported the rheology and chain dynamics including the tumbling motion and relaxation using the Brownian dynamics (BD) simulation. Recently, Usta *et al.* (2005) examined the effect of confined flow on the distribution of polymer chains using the Lattice-Boltzmann simulation, and found that the polymer migrates to the center of the channel due to hydrodynamic interaction. Fang *et al.* (2005) measured DNA stretch as a function of distance from the wall. The molecules were compressed to the direction perpendicular to the wall in the vicinity of the wall regardless of the flow

*Corresponding author: ahnnet@snu.ac.kr

strength but they stretched as the distance from the wall increases at stronger flow.

However, many studies were limited to the polymer dynamics in the prescribed velocity field. For better control and design of the microfluidic devices, it will be important to have a clear understanding on the flow behavior of polymers in the complex flow fields. In this study, we investigate the orientation and deformation of polymers in a channel flow as well as in the complex flow using the micro-macro simulation technique that can consider the interaction between the fluid flow and polymer dynamics. To take the wall effect in the confined channel flow into account, we apply the anisotropic drag and anisotropic Brownian force that lead to the increased mobility toward the flow direction near the wall. Even though more rigorous modeling will be required for better description of the interactions between the wall and polymers, we have compromised to introduce the concept of anisotropy to reduce the computational burden, while taking the interaction of flow field and polymer dynamics into account. We will describe not only average but individual configurations of polymers near the wall at the same time.

This paper is organized as follows. The basics of molecular modeling and the governing equations with spatial constriction are introduced in Section 2. The numerical algorithm and the conditions for numerical simulation are presented in Section 3. The algorithm verification in the simple shear flow and the simulation results in both Poiseuille flow and 4 : 1 contraction flow are discussed in Section 4, with particular emphasis on the molecular tumbling behavior that is observed close to the wall under strong anisotropic drag and high shear flow region. And the concluding remarks will be followed in Section 5.

2. Governing equations

As a polymer consists of many repeating units, it is common to model the polymer chain as a series of beads connected by springs or rods. The simplest but very efficient method is to model the polymer as a dumbbell; two beads are connected by a spring. Depending on the character of the spring and the molecular concepts for diverse interactions between the components, there arise many molecular models for polymer dynamics. In this work, we model the polymer solution as a suspension of finitely extensible nonlinear elastic (FENE) dumbbells. In this model, the spring force is linear at small extensions, but the spring becomes stiffer as it is more extended. The configuration of FENE dumbbell can be described by a connector vector $\boldsymbol{Q}$ which connects two beads of a dumbbell, and the FENE spring force is expressed as follows (Bird *et al.*, 1987),

$$\boldsymbol{F}^{(c)} = \frac{H\boldsymbol{Q}}{1-(Q/Q_0)^2},\ Q \le Q_0, \tag{1}$$

where H is the spring constant and Q_0 is the maximum extensible length of the connector vector $\boldsymbol{Q}$. This equation means that the spring cannot be extended beyond a maximum separation Q_0 because there exists a mathematical singularity when $Q = |\boldsymbol{Q}| = Q_0$.

In the absence of an external force, the force balance for each bead n of a dumbbell consists of a hydrodynamic drag force $\boldsymbol{F}_\nu^{(h)}$, a Brownian force $\boldsymbol{F}_\nu^{(b)}$, and an intramolecular force $\boldsymbol{F}_\nu^{(\phi)}$;

$$\boldsymbol{F}_\nu^{(h)} + \boldsymbol{F}_\nu^{(b)} + \boldsymbol{F}_\nu^{(\phi)} = 0. \tag{2}$$

If we assume that the perturbation of the flow field at one bead resulting from the motion of the other bead is negligible and the friction tensor is isotropic $\zeta = \zeta \boldsymbol{I}$, Eq. (2) becomes

$$-\zeta([\boldsymbol{r}_\nu] - \nu_0 - [\boldsymbol{k}\cdot\boldsymbol{r}_\nu]) - k_B T \frac{\partial}{\partial \boldsymbol{r}_\nu} \ln\psi + \boldsymbol{F}_\nu^{(\phi)} = 0,\ (\nu = 1,2) \tag{3}$$

where $\boldsymbol{k}$ is the velocity gradient tensor, $\boldsymbol{r}_\nu$ is the position vector of bead ν, and ψ is the configuration-space distribution function. The subtraction of the two equations about each bead makes the equation of motion for the dumbbell connector vector $\boldsymbol{Q} = \boldsymbol{r}_1 - \boldsymbol{r}_2$. Then we can get a diffusion equation from the equation of continuity for $\psi(\boldsymbol{Q},t)$,

$$\frac{\partial \psi}{\partial t} = -\left(\frac{\partial}{\partial \boldsymbol{Q}} \cdot \left\{ [\boldsymbol{k}\cdot\boldsymbol{Q}]\psi - \frac{2k_BT}{\zeta}\frac{\partial}{\partial \boldsymbol{Q}}\psi - \frac{2}{\zeta}\boldsymbol{F}^{(c)}\psi \right\} \right). \tag{4}$$

In microchannel flow, the motion of the dumbbells is strongly affected by the wall when the characteristic length of the geometry is small. We introduce anisotropic drag to take this spatial restriction by the wall into account for simplicity, although long range hydrodynamic interaction should be taken into account for rigorous calculation. The mobility of a dumbbell towards the wall direction is strongly suppressed near the wall. So we assume that the inverse friction tensor $\zeta^{-1}(x)$ is anisotropic to account for the anisotropic mobility of the dumbbell (Bird and Deaguiar, 1983; Bird and Wies, 1984). Because the mobility of a dumbbell may vary according to the position in the microchannel, we simply assume that the degree of anisotropy has its position dependence in the form of an exponential function,

$$\zeta^{-1}(x) = \frac{1}{\zeta}[(1-\alpha(x))\boldsymbol{I} + \alpha(x)\boldsymbol{u}\boldsymbol{u}]. \tag{5}$$

Vector $\boldsymbol{u} = \boldsymbol{Q}/|\boldsymbol{Q}|$ is the unit vector in the direction of the connector vector $\boldsymbol{Q}$, and $\alpha(x)$ is the anisotropy parameter and has the value between 0 and 1,

$$\alpha(x) = \alpha_{wall}\frac{\exp(x/L)-1}{\exp(1)-1}. \tag{6}$$

L is the half of the channel width and x is the distance away from the symmetry line. In the case of $x=0$ (sym-

metry line), α equals zero, which means the mobility to all directions is the same. As the position moves to the wall, α increases exponentially, which means the mobility toward the connector vector direction becomes dominant, and for the extreme case of $x=L$ at the wall, α becomes α_{wall} (we set α_{wall} to be 0.99) and the mobility of the dumbbell is totally toward the connector vector direction. The concept of anisotropic drag is also used to model the entanglements in concentrated solutions or melts, leading to the encapsulated dumbbell model or the Giesekus model. Even though the concept is similar, the origin of anisotropy (one from the wall effect and the other from the entanglement) and the system (one is dilute suspension of dumbbells and the other is concentrated solutions or melts) are quite different. Here, the beads close to the wall may pass through the wall because the center of the dumbbell can be located at the wall of the Eulerian grid in the Brownian configuration fields, which will be explained later.

Using the anisotropic friction tensor, we can derive a new Fokker-Planck equation (Deaguiar, 1983; Baxandall, 1987; Biller and Petruccione, 1988).

$$\frac{\partial \psi}{\partial t} = -\left(\frac{\partial}{\partial \boldsymbol{Q}} \cdot \left\{ [\boldsymbol{k}\cdot\boldsymbol{Q}]\psi - 2k_BT\zeta^{-1}\cdot\frac{\partial}{\partial \boldsymbol{Q}}\psi - 2\zeta^{-1}\cdot\boldsymbol{F}^{(c)}\psi \right\}\right) \tag{7}$$

The Fokker-Planck equation can be transformed into an equivalent stochastic differential equation for the connector vector $\boldsymbol{Q}$ by Langevin approach as follows (Öttinger, 1996),

$$\boldsymbol{Q}(t+\Delta t) = \boldsymbol{Q}(t) + \Delta t\Big[\boldsymbol{k}\cdot\boldsymbol{Q}(t) - 2\zeta^{-1}(x,t)\cdot\boldsymbol{F}^{(c)}(t) + \\ + 2k_BT\Big(\frac{\partial}{\partial \boldsymbol{Q}}\cdot\zeta^{-1}(x,t)\Big)(t)\Big] + \sqrt{\Delta t}\boldsymbol{A}(x,t)\cdot f(t), \tag{8}$$

where $\boldsymbol{A}\cdot\boldsymbol{A}^T = 4k_BT\zeta^{-1}$, $\boldsymbol{A}$ can be obtained by Cholesky decomposition of ζ^{-1} and the components of f are Gaussian random numbers with zero mean and unit variance. In Eq. (8), the inverse friction tensor $\zeta^{-1}(x,t)$ and the tensor $\boldsymbol{A}(x,t)$ can be updated from $\boldsymbol{Q}(t)$ for each time step, but the velocity gradient tensor $\boldsymbol{k}$ should be specified analytically or be solved from the conservation equations.

Here we choose the latter and couple the conservation equations with the stochastic equations for dumbbell model by using CONNFFESSIT (Calculation Of Non-Newtonian Flow: Finite Elements and Stochastic Simulation Technique) approach, which uses stochastic simulation from the molecular kinetics explained above as an alternative to the traditional constitutive equation for the simulation of viscoelastic flows. We used the Brownian configuration field method of Eulerian approach among the CONNFFESSIT-type methods to circumvent individual dumbbell tracking, by introducing spatially continuous, convected and deformed Brownian configuration fields. In the Brownian configuration field method, the connector vector $\boldsymbol{Q}(t)$ is replaced by the spatially continuous Brownian configuration field $\boldsymbol{Q}(x,t)$ (Hulsen *et al.*, 1997; Öttinger *et al.*, 1997; Somasi and Khomami, 2000). For the convenience of calculation, non-dimensionalized variables and parameters are introduced to the governing equations, then the non-dimensionalized governing equation becomes

$$\boldsymbol{Q}(x,t+\Delta t) = \boldsymbol{Q}(x,t) + \frac{1}{\sqrt{Wi}}\boldsymbol{A}(x,t)\cdot\Delta\boldsymbol{W}(t) \\ + \Delta t\Big[-\boldsymbol{v}\cdot\nabla\boldsymbol{Q}(x,t) + \boldsymbol{k}\cdot\boldsymbol{Q}(x,t) - \frac{1}{2Wi}\zeta^{-1}(x,t)\cdot\boldsymbol{F}^{(c)}(x,t) \\ + \frac{1}{2Wi}\Big(\frac{\partial}{\partial \boldsymbol{Q}}\cdot\zeta^{-1}\Big)(x,t)\Big] \tag{9}$$

Here $\boldsymbol{Q}$ is now non-dimensionalized by $\sqrt{k_BT/H}$, $\boldsymbol{v}$ denotes the dimensionless velocity vector. The *Weissenberg* (*Wi*) number is defined by $\lambda V/L$ where V is the characteristic velocity, L is the characteristic length, and the relaxation time λ is defined by $\zeta/4H$. $\Delta\boldsymbol{W}$ refers the Wiener process of Gaussian random numbers with zero mean and Δt variance. Spring force of FENE is also non-dimensionalized as follows,

$$\boldsymbol{F}^{(c)} = \frac{\boldsymbol{Q}}{1-Q^2/b}. \tag{10}$$

Nonlinear parameter $b=HQ_0^2/(k_BT)$ is a dimensionless constant that relates to the maximum extensibility of a dumbbell. The inverse friction tensor is modified as in Eq. (11),

$$\zeta^{-1} = (1-\alpha)\boldsymbol{I} + \alpha\boldsymbol{u}\boldsymbol{u}, \tag{11}$$

where $\boldsymbol{A}$ is obtained from $\boldsymbol{A}\cdot\boldsymbol{A}^T=\zeta^{-1}$. The polymeric stress of dumbbells can be obtained by the ensemble average of the Brownian configuration fields using the Kramer's expression

$$\tau_p(x,t) = \frac{(1-\beta)}{Wi^*}\Big(-\boldsymbol{I} + \frac{1}{N_d}\sum_{i=1}^{N_d}\boldsymbol{Q}_i(x,t)\boldsymbol{F}_i^{(c)}(x,t)\Big),\ Wi^* = \frac{Wi}{1+5/b}, \tag{12}$$

where N_d is the number of dumbbells to be ensemble averaged at each node, $\beta=\eta_s/\eta_0=\eta_s/(\eta_s+\eta_p)$ is the ratio of the solvent viscosity to the total viscosity, and $\boldsymbol{Q}_i(x,t)$ represents the Brownian configuration field of the i^{th} dumbbell used in the ensemble average.

The isothermal flow of incompressible polymer solution is governed by the momentum balance equation and the continuity equation. For the conservation equations, we assume the creeping flow and use the discrete elastic viscous split stress (DEVSS-G) scheme in the formulation of the finite element method to stabilize the governing equations as follows,

$$-\nabla p + \nabla\cdot\boldsymbol{\tau}_p + \nabla^2\boldsymbol{v} - (1-\beta)\nabla\cdot\boldsymbol{k} = 0 \\ \boldsymbol{k} - (\nabla\boldsymbol{v})^T = 0, \\ \nabla\cdot\boldsymbol{v} = 0 \tag{13}$$

where p is the fluid pressure. A polymeric stress τ_p

obtained from the above stochastic process can be coupled with the flow field.

3. Numerical scheme and simulation conditions

For the spatial discretisation, we used the finite element method in both Brownian configuration field and the conservation equations. For the Brownian configuration field, the use of semi-implicit predictor-corrector method proposed by Öttinger (1996) makes the FENE dumbbells avoid unphysical condition of $\boldsymbol{Q}(|\boldsymbol{Q}|^2 > b)$. But the corrector step of that scheme has different stiffness matrix at each time step, and it makes computing time exorbitant. To remove this difficulty, we applied the semi-implicit predictor-corrector method only for the dumbbells having unphysical configurations so that we could achieve high computational efficiency with little loss of accuracy,

(1) *predictor step*

$$\boldsymbol{Q}_j^{n+1^*} = \boldsymbol{Q}_j^n + \Big[-\boldsymbol{v}^n \cdot \nabla \boldsymbol{Q}_j^n + \boldsymbol{k}^n \cdot \boldsymbol{Q}_j^n - \frac{1}{2Wi}(\zeta^1 \cdot \boldsymbol{F}^{(c)})_j^n + \frac{1}{2Wi}\Big(\frac{\partial}{\partial \boldsymbol{Q}} \cdot \zeta^1\Big)_j^n \Big]\Delta t + \frac{1}{\sqrt{Wi}}(\boldsymbol{A} \cdot \Delta \boldsymbol{W})_j^n$$

(2) *corrector step*

$$\boldsymbol{Q}_j^{n+1} = \boldsymbol{Q}_j^n + \Big[-\boldsymbol{v}^n \cdot \nabla \boldsymbol{Q}_j^n + \boldsymbol{k}^n \cdot \boldsymbol{Q}_j^n - \frac{1}{2Wi}(\zeta^1 \cdot \boldsymbol{F}^{(c)})_j^n + \frac{1}{2Wi}\Big(\frac{\partial}{\partial \boldsymbol{Q}} \cdot \zeta^1\Big)_j^n \Big]\Delta t + \frac{1}{2}\Big[-\boldsymbol{v}^{n+1} \cdot \nabla \boldsymbol{Q}_j^{n+1^*} + \boldsymbol{k}^{n+1} \cdot \boldsymbol{Q}_j^{n+1^*} - \frac{1}{2Wi}(\zeta^1 \cdot \boldsymbol{F}^{(c)})_j^{n+1^*} + \frac{1}{2Wi}\Big(\frac{\partial}{\partial \boldsymbol{Q}} \cdot \zeta^1\Big)_j^{n+1^*} \Big]\Delta t + \frac{1}{2\sqrt{Wi}}[(\boldsymbol{A} \cdot \Delta \boldsymbol{W})_j^n + (\boldsymbol{A} \cdot \Delta \boldsymbol{W})_j^{n+1^*}]$$

if $|\boldsymbol{Q}_j^{n+1}|^2 > b$ *goto* (3)

(3) *semi-implicit corrector step*

$$\Big(1 - \frac{1}{4Wi}\frac{\Delta t}{1 - (\boldsymbol{Q}_j^2)^{n+1}/b}\zeta^1 \cdot\Big)\boldsymbol{Q}_j^{n+1} = \boldsymbol{Q}_j^n + \frac{1}{2}\Big[-\boldsymbol{v}^n \cdot \Delta \boldsymbol{Q}_j^n + \boldsymbol{k}^n \cdot \boldsymbol{Q}_j^n - \frac{1}{2Wi}(\zeta^1 \cdot \boldsymbol{F}^{(c)})_j^n + \frac{1}{2Wi}\Big(\frac{\partial}{\partial \boldsymbol{Q}} \cdot \zeta^1\Big)_j^n \Big]\Delta t + \frac{1}{2}\Big[-\boldsymbol{v}^{n+1} \cdot \nabla \boldsymbol{Q}_j^{n+1^*} + \boldsymbol{k}^{n+1} \cdot \boldsymbol{Q}_j^{n+1^*} + \frac{1}{2Wi}\Big(\frac{\partial}{\partial \boldsymbol{Q}} \cdot \zeta^1\Big)_j^{n+1^*} \Big]\Delta t + \frac{1}{2\sqrt{Wi}}[(\boldsymbol{A} \cdot \Delta \boldsymbol{W})_j^n + (\boldsymbol{A} \cdot \Delta \boldsymbol{W})_j^{n+1^*}], \quad (14)$$

where the superscript n, $n+1$, and asterisk stand for the variables of present step, next step and predictor variables of the next step, respectively. In the semi-implicit corrector step in the above adaptive scheme, Eq. (14), we can get a cubic equation

$$x^3 - Rx^2 - \Big(1 + \frac{\Delta t}{4Wi}\Big)bx + Rb = 0 \quad (15)$$

where $x = |\boldsymbol{Q}^{n+1}|$, R is the right-hand side term of the third step of Eq. (14). Eq. (15) has a solution between 0 and $\sqrt{b}$, so unphysical configuration of FENE dumbbell can be avoided.

We used bilinear polynomials as the interpolation functions for the Brownian configuration fields. The discontinuous Galerkin (DG) formulation was used to stabilize the hyperbolic character in the stochastic differential equation of the Brownian configuration field. Also, we performed parallel computing which distributes the configuration fields to the processors using the Massage Passing Interface (MPI). In solving Eq. (13), we used biquadratic polynomials for the velocity field, and bilinear polynomials for the pressure and velocity gradient tensor as interpolation functions. The conservation equations were solved serially because the dominant time-consuming step was the solution step of the Brownian configuration fields. The advantage of this algorithm, which solves velocity field and polymer stress self-consistently, consists of 1) it provides information for both flow field and polymer dynamics, 2) it considers the interaction between fluid and polymer, 3) it can solve chain dynamics in complex flow fields, 4) computationally effective and 5) many polymer chains (dumbbells) can be incorporated (dramatic when compared with Stokesian dynamics simulation).

Two different geometries were used in this study. One is planar channel and the other is 4:1 planar contraction. The former is to investigate the effect of various conditions on the polymer configuration, while the latter is to investigate the polymer configurations in complex flow fields. In the mesh of planar channel, the number of elements was 300, and the degree of freedom (DOF) of conservation equations was 4,222. After the parameter study in the Poiseuille flow, we applied this algorithm to the 4:1 planar contraction geometry to investigate the dumbbell configurations in complex flow fields. The number of elements was 1,985 and DOF of conservation equations was 26,802. The number of the Brownian configuration fields used for the ensemble average was 2,000 per node and we set the dimensionless time step $\Delta t = 0.001$. The stochastic error in the steady state solution was found to be less than 8% of the mean stress value.

4. Results and discussion

In order to verify the reliability of the algorithm, we first compared our result with the previous report of Biller and Petruccione (1988) under constant anisotropic drag coefficient, in which the Brownian dynamics simulation was

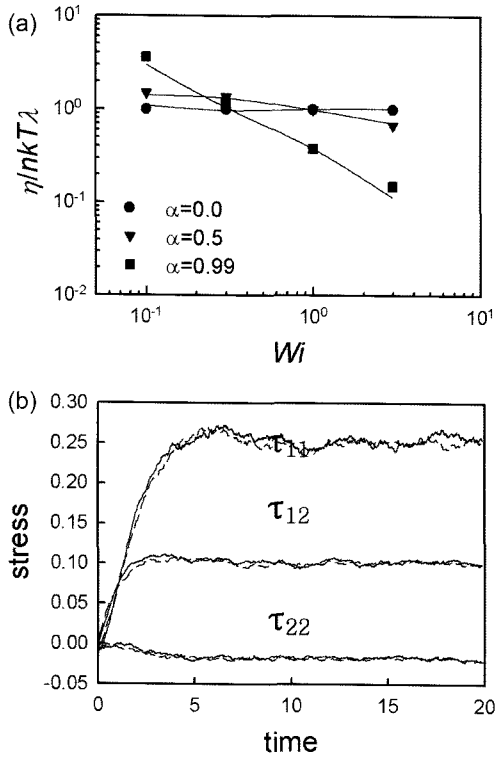

Fig. 1. (a) Shear viscosity of Hookean elastic dumbbell (lines) compared with Biller and Petruccione' work (ref. 18; symbols) as a function of Wi at various anisotorpic parameters; $\beta=0$; (b) simulation results by Brownian configuration field method (solid line) and by Brownian dynamics simulation (dashed line); $Wi=1$, $\beta=0.9$, $\alpha=0.5$.

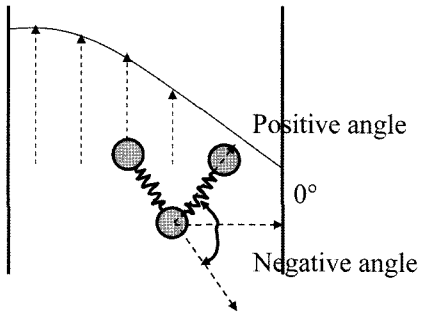

Fig. 2. Definition of orientation angle.

performed with the Hookean elastic dumbbell model in simple shear flow. Fig. 1(a) shows the shear viscosity vs. Wi. The results from the Brownian dynamics simulation agree well, with some deviations which are within statistical error tolerance. The robustness of the Brownian configuration field method is also supported in Fig. 1(b), in which good agreement can be found in the start-up behavior of simple shear flow. The agreement between the predictions from different algorithms in spite of the stochastic nature confirms the reliability of the algorithm suggested in the previous section. We now change the elastic spring force to more realistic FENE spring force.

We performed a parameter study to understand the effect of flow conditions and polymer characteristics on the orientation and stretching of FENE dumbbells in the Poiseuille flow. The average orientation angle (ϕ) and average stretching (S) of FENE dumbbells are defined by the

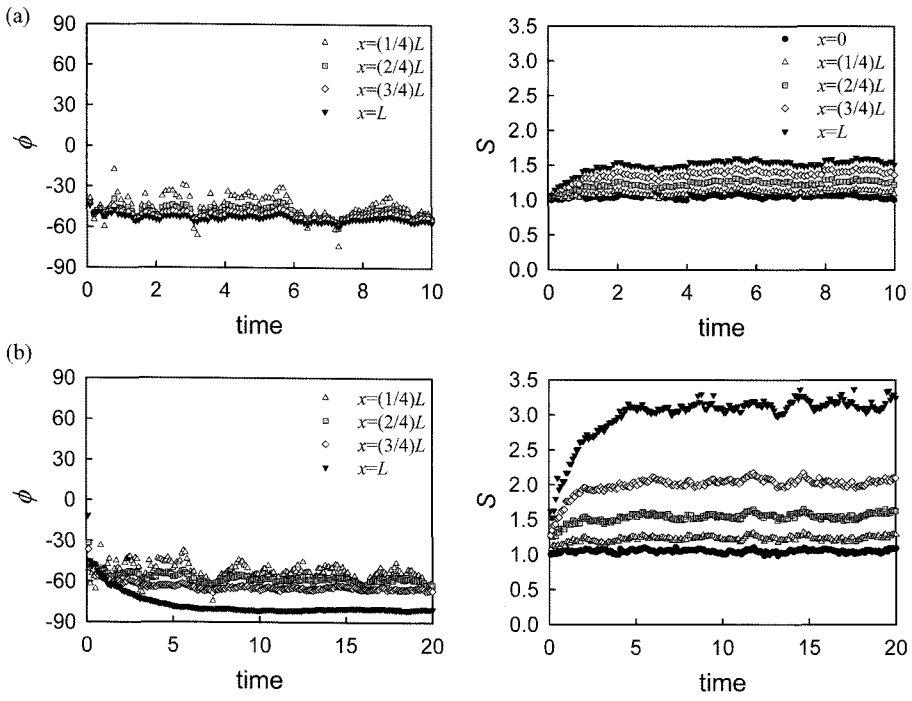

Fig. 3. Average orientation and stretching of dumbbells as a function of position in a channel when (a) isotropic drag and (b) anisotropic drag are imposed respectively; $Wi=0.5$, $\beta=0.9$, $b=100$.

ensemble average over 2,000 Brownian configuration fields. We take the ensemble average $\langle \boldsymbol{QQ} \rangle$ of Brownian configuration fields, from which two principal axes are obtained by solving the eigenvalue problem. Then the direction of the major principal axis is defined as the average orientation direction, and the average stretching is defined by the length of the major principal axis of $\langle \boldsymbol{QQ} \rangle$ divided by its equilibrium length. The orientation angle 0° means that the dumbbell aligns perpendicular to the flow direction. The positive sign in the orientation angle is the counter-clockwise direction, and the negative sign is the clockwise direction from the 0° axis as shown in Fig. 2. The orientation angle lies in the range of $-90° \sim +90°$. Ultimately $-90°$ and $+90°$ represent the same orientation, that is, the alignment of dumbbells with the flow direction.

The average configurations of FENE dumbbells in a channel are shown in Fig. 3 with isotropic and anisotropic drag, where the position $x=0$ denotes the symmetry line where the velocity gradient is zero, and the position $x=L$ denotes the wall where the velocity gradient becomes the maximum. They are used simply for convenience to indicate the position in the flow domain. In both cases, the FENE dumbbells at the symmetry line show random orientation due to the Brownian motion, but in the shear flow region away from the center they align to the flow direction with larger angle and the dumbbells stretch more as they come closer to the wall. The difference between isotropic and anisotropic drag becomes clearer near the wall. When the anisotropic drag is imposed, the polymers more orient and more stretch. Near the wall, it takes longer time to reach the steady state than other cases. Anisotropic drag caused by the wall interaction in a channel makes dumbbells more align to the flow direction and stretch because the mobility to the flow direction becomes more pronounced and the orthogonal motion is suppressed.

The configuration of dumbbells can be affected by parameters relating to the flow conditions. We performed parameter studies to understand the influence of viscosity ratio, shear rate and maximum extensibility of FENE dumbbells in planar channel flow. The orientation and stretch of FENE dumbbells depend not only on the flow conditions but also on the position where the dumbbell is located within the channel. From now on, we will compare the configurations of FENE dumbbells near the wall (at the fixed position $x=3.88L/4$), to remove the position-dependence of the configurations. In Fig. 4(a), the average orientation angle is rarely affected by these parameters. But as far as the average stretching is concerned, lower *Wi* and lower maximum extensibility reduce the degree of stretching of dumbbells quite significantly in Fig. 4(b). The velocity profile is almost the same with the Newtonian parabolic profile but deviates as β changes. It slightly changes from parabolic ($\beta=0.9$) to bell-shaped profile ($\beta=0.5$) as in Fig. 4(c). Near the wall, the velocity change is small but the

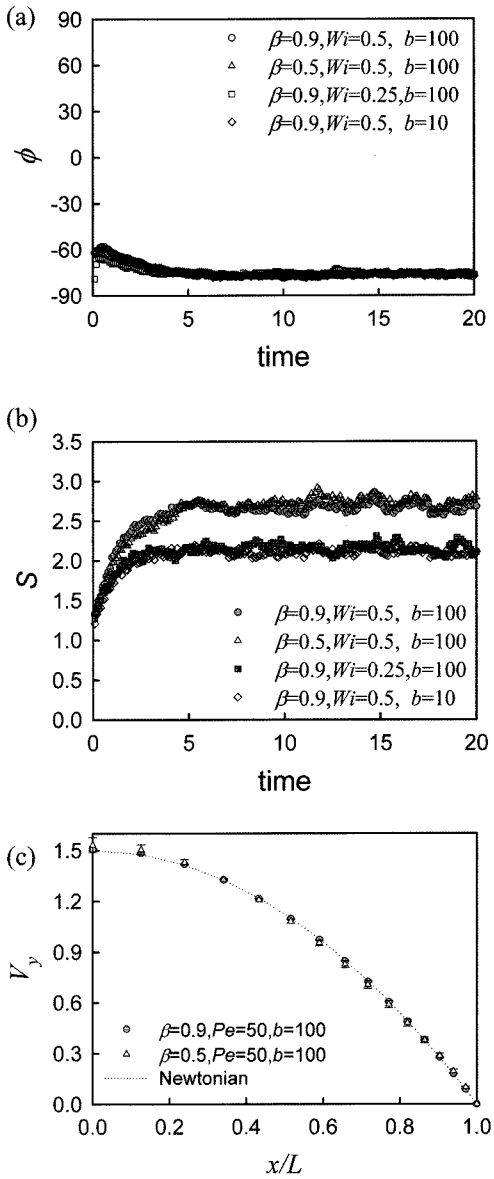

Fig. 4. Effect of viscosity ratio, *Wi*, and the maximum extensibility of FENE dumbbells on (a) average orientation, (b) stretching of dumbbells, and (c) velocity profiles.

shear rate slightly increases when the polymer contribution increases, which affects the average stretch as in Fig. 4(b).

Of particular interest is the tumbling of molecules (Smith *et al.*, 1999; Woo *et al.*, 2004b; Teixeira *et al.*, 2005; Schroeder *et al.*, 2005). We could observe tumbling of individual dumbbell and the tumbling was outstanding near the wall. The orientation angles of some FENE dumbbells are shown in Fig. 5. We observe random orientation at the symmetry line, but near the wall at $x=3.88L/4$ some individual molecules undergo tumbling motion as shown in Fig. 5(b) although they have random orientation near the wall in the case of isotropic drag. At the position at $x=3L/4$ in Fig. 5(a), the tumbling of dumbbells appears more frequently and the number of dumbbells having random ori-

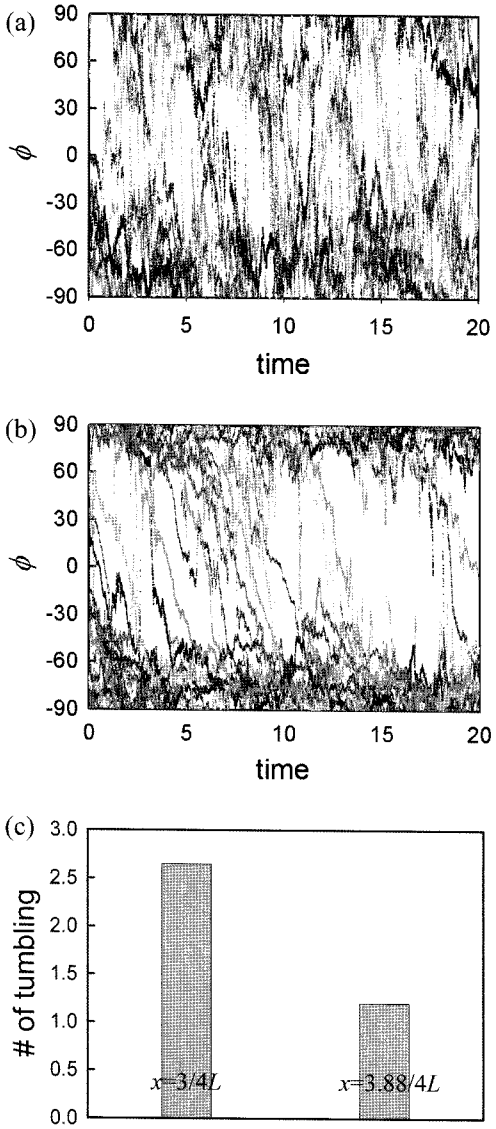

Fig. 5. Orientation of individual FENE dumbbells at, (a) $x=3L/4$, (b) $x=3.88L/4$ and (c) average number of tumbling per dumbbell for $t=20$; $Wi=0.5$, $\beta=0.9$, $b=100$.

entation becomes larger than near the wall. Average number of tumbling per a dumbbell during the simulation time is also given in Fig. 5(c). However, there was no apparent cyclic dynamics related to molecular tumbling as reported in the previous studies (Teixeira *et al.*, 2005; Schroeder *et al.*, 2005).

This particular behavior is now to be discussed in terms of the dominating forces and their roles. If we only consider the effect of flow field on the dumbbell configuration and if the individual molecule is aligned with negative angle, the dumbbell extends and aligns more along the flow direction as in Fig. 6(a) because the bead far from the wall moves faster than the bead close to the wall. The dumbbells whose orientation angles are near $-90°$ can sometimes fluctuate to the positive angles due to the

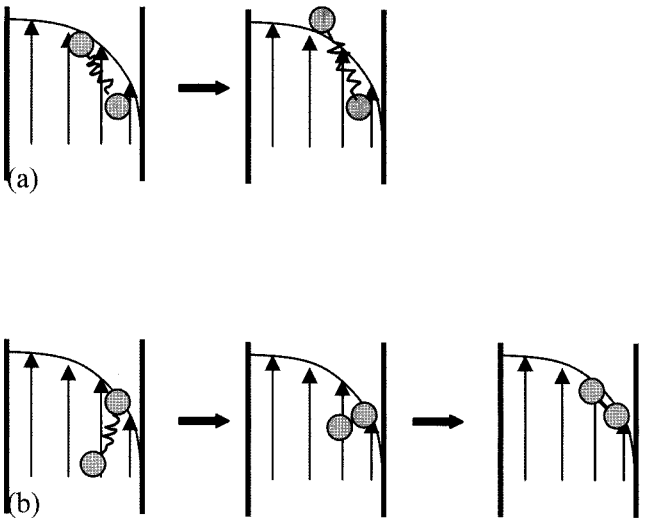

Fig. 6. Effect of ambient flow field on the configuration of FENE dumbbells; (a) stretching and alignment, (b) shrinkage and tumbling.

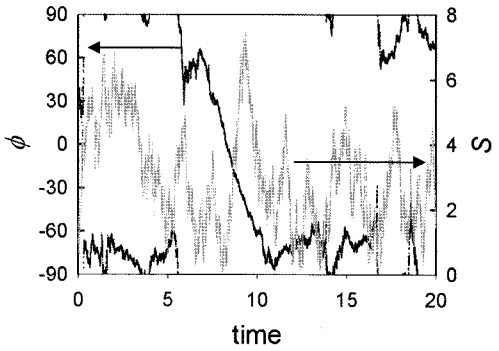

Fig. 7. Orientation angle and stretching of a dumbbell near the wall; $Wi=0.5$, $\beta=0.9$, $b=100$.

Brownian motion. If a molecular configuration has a positive orientation angle, the molecule tumbles over and stretches again as in Fig. 6(b). So the probability of tumbling becomes higher near the wall because the velocity gradient is larger near the wall than far from the wall. But, the dumbbell configuration is not affected by the flow field alone. When we observe the orientation and stretching of the individual dumbbell as in Fig. 7, they seem to be affected in a complex way by the flow field, spring force, and Brownian force rather than simple mechanism of stretching and alignment (Fig. 6(a)) or shrinkage and tumbling (Fig. 6(b)). To tumble over, the dumbbells should occasionally have positive angles by Brownian force. Then, they experience shrinkage and tumbling at high shear rate through the mechanism of Fig. 6(b). In other words, the Brownian force plays a role as a cause of tumbling and high shear rate facilitates it. In addition, the anisotropic drag near the wall makes dumbbells more stretch and align than the isotropic drag at the symmetry

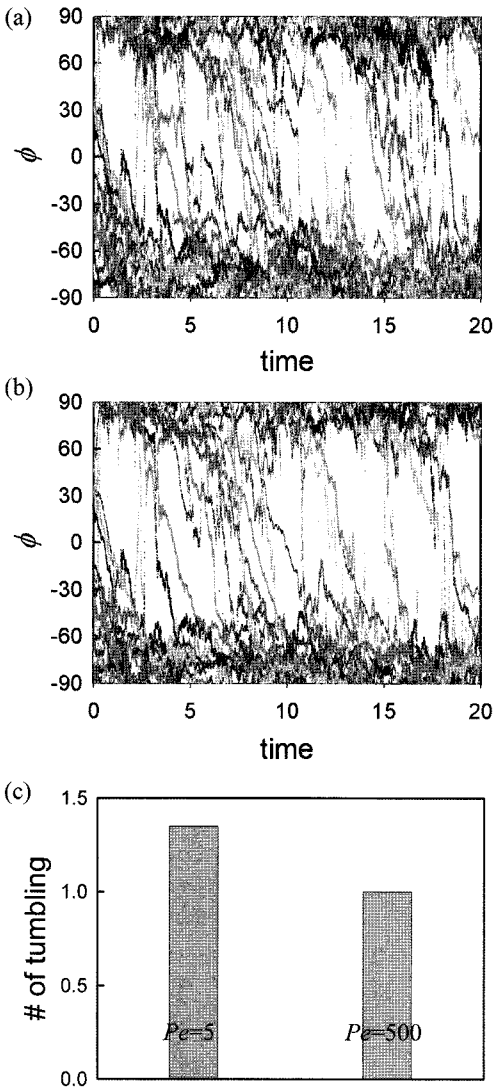

Fig. 8. Effect of *Pe* on the individual tumbling of FENE dumbbells; (a) *Pe*=5, (b) *Pe*=500 (c) average number of tumbling per dumbbell for t=20; Wi=0.5, β=0.9.

line, while anisotropic Brownian force makes the Brownian motion act along the dumbbell direction. These anisotropic effects facilitate tumbling as well as stretching and alignment. Tumbling was seldom observed under isotropic drag at the symmetry line, because the dumbbells less stretch and align compared to the case with anisotropic drag and they have random orientation due to isotropic Brownian force that disturbs tumbling. Next, we investigated the relationship among the acting forces on the dumbbells to understand the effects of the governing forces on molecular tumbling. Here we define the *Peclet* number (*Pe*) as the shear rate ($\dot{\gamma}$) multiplied by the characteristic time for the Brownian motion (τ_{Brown}).

$$Pe = \dot{\gamma}\tau_{Brown} = \dot{\gamma}\frac{\zeta Q_0^2}{4kT} = \dot{\gamma}\frac{\zeta b}{4L} = \dot{\gamma}\lambda b = Wi \cdot b \tag{16}$$

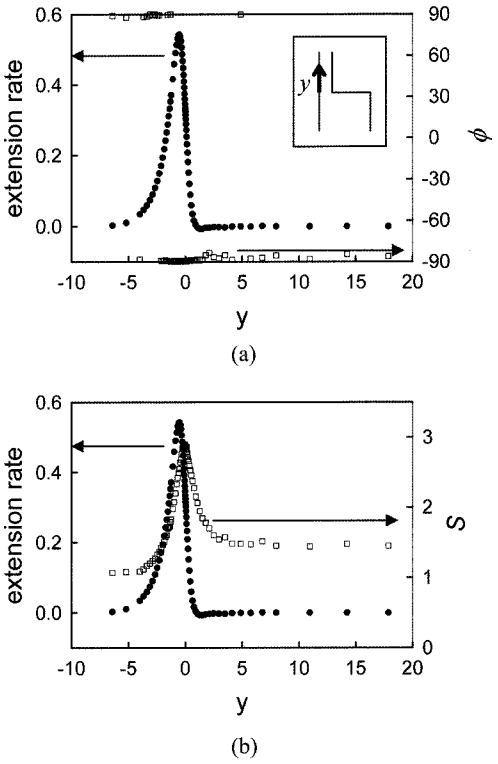

Fig. 9. (a) Orientation and (b) stretching of FENE dumbbells with extensional rate along the center line in the extensional flow region of 4 : 1 planar contraction flow near the reentrance; Wi=0.5, β=0.9, b=100; y=0 denotes the reentrant position.

We examined the effect of *Pe* on tumbling in Fig. 8. At low *Pe*, even though some dumbbells have positive angles, many of them still have a tendency to keep the random orientation because shear force is not strong enough to induce tumbling compared to the Brownian force. On the other hand at high *Pe*, the dumbbells keep on tumbling once they have positive angles because the flow field is strong enough to overweigh the restoring force to the random orientation. However, the number of dumbbells that undergo tumbling is smaller at high *Pe* because the dumbbells have less chance to align to the positive angle due to the relatively weak Brownian force.

The degree of anisotropic drag has been used as the form of Eq. (6), but on the other hand the exponential form of anisotropy may not be accurate and we have also checked the sensitivity of α_{wall}. As α_{wall} varies from 0.9 to 0.99, the dumbbell configuration changes only close to the wall. The average orientation angle differs by 3.9% for α_{wall}=0.95, and 7.0% for α_{wall}=0.9 compared to the case of α_{wall}=0.99. And the change of average stretch is 3.8% for α_{wall}=0.95 and 7.3% for α_{wall}=0.9. The effect of alpha is more pronounced in the motion of individual dumbbell. The number of tumbling of a dumbbell during 20 time units differs by less than 8.3% for α_{wall} larger than 0.95, while it differs significantly for α_{wall}=0.9. The dynamics (whether individual

or average) does not change significantly provided that α_{wall} is larger than 0.95.

Contraction flow is frequently encountered in many flow devices. In contraction flow, the extensional flow is dominant along the symmetry line near the contraction, and the polymer configuration in this region differs from that in Poiseuille flow. We performed simulation of 4 : 1 planar contraction flow with the same flow rate used in the Poiseuille flow above. We plotted average orientation angle as well as the average degree of stretching together with the extension rate along the symmetry line in Fig. 9. The extension rate was defined as $\partial v_y/\partial y$. The extension rate increases along the symmetry line and reaches maximum before the reentrant region ($y=0$), and decreases afterwards while the dumbbells stretch and relax. But there exists some time lag. The dumbbells relax slowly after the extensional flow region being not completely relaxed afterwards. In other words, the memory is not eliminated completely after passing through the extensional flow region. Moreover, the dumbbells in extensional flow region keep their alignment along the flow direction from the extensional flow region to the end of the channel. The individual FENE dumbbells in the extensional flow region undergo quicker and more frequent tumbling compared to shear flow. The extensional flow is so strong that the dumbbells more align to the flow direction, and are influenced by random Brownian force that is isotropic in this region. In the shear flow, on the other hand, the flow is less strong and the Brownian force is anisotropic near the wall. Therefore, the dumbbell configuration is determined not only by the wall interaction but also by the flow type such as shear or extension resulting from the geometric origin.

5. Conclusions

In this study, we investigated the polymer configuration in both simple shear and complex flow field by modeling the dilute polymer solution as a suspension of FENE dumbbells. By using the micro-macro approach, we could obtain the average macroscopic configuration as well as the individual configuration of each polymer chain at the same time. In particular, the anisotropic drag and anisotropic Brownian motion were considered in order to model the interaction between the polymer and the wall in a confined channel flow. Molecular tumbling was observed near the wall, and we investigated the mechanism of tumbling behavior in terms of the acting forces. It was strongly influenced by anisotropic drag and high shear close to the wall. We discussed the mechanism of this particular behavior in terms of *Pe* which is the ratio of shear force and Brownian force. At high *Pe*, the dumbbells keep on tumbling once they have positive angles, but the number of dumbbells that undergo tumbling is reduced. The dumbbell configuration could be determined not only by the wall interaction but also by the flow type such as shear or extension resulting from the geometric origin. In the contraction flow, the memory was not eliminated completely even after passing through the extensional flow region. The dumbbells keep their alignment along the flow direction from the extensional flow region to the end of the channel and they are not completely relaxed after stretching. The individual FENE dumbbells in the extensional flow region of 4 : 1 contraction flow undergo quicker and more frequent tumbling because the dumbbells more align to the flow direction and are influenced by random Brownian force.

Acknowledgements

This work was supported by the National Research Laboratory Fund (M10300000159) of the Ministry of Science and Technology in Korea. The authors acknowledge the support from KISTI (Korea Institute of Science and Technology Information) under 'Grand Challenge Support Program' with Dr. Jeong Ho Kim as the technical supporter. The use of the computing system of Supercomputing Center is also greatly appreciated.

References

Baxandall, L.G., 1987, Anisotropic friction in polymeric models I. The elastic dumbbell and reptating chain, *J. Chem. Phys.* **87**, 2297-2304.

Biller, P. and F. Petruccione, 1988, Rheological properties of polymer dumbbell models with configuration-dependent anisotropic friction, *J. Chem. Phys.* **89**, 2412-2418.

Bird, R.B., R.C. Armstrong and O. Hassager, 1987, Dynamics of Polymeric Liquids Vol. 2., Wiley, New York.

Bird, R.B. and J.R. Deaguiar, 1983, An encapsulated dumbbell model for concentrated polymer solutions and melts I. Theoretical development and constitutive equation, *J. Non-Newt. Fluid Mech.* **13**, 149-160.

Bird, R.B. and J.M. Wies, 1984, Anisotropic effects in dumbbell kinetic theory, *J. Rheol.* **29**, 519-532.

Deaguiar, J.R., 1983, An encapsulated dumbbell model for concentrated polymer solutions and melts II. Calculation of material functions and experimental comparisons, *J. Non-Newt. Fluid Mech.* **13**, 161-179.

Doyle, P.S., G. Ladoux and J. Viovy, 2000, Dynamics of a tethered polymer in shear flow, *Phys. Rev. Lett.* **84**, 4769-4772.

Fang, L., H. Hu and R.G. Larson, 2005, DNA configurations and concentraction in shearing flow near a glass surface in a microchannel, *J. Rheol.* **49**, 127-138.

Hoagland, D.A. and R.K. Prud'homme, 1988 , Molecular shape in homogeneous flows: predictions of the Rouse model, *J. Non-Newt. Fluid Mech.* **27**, 223-243.

Hulsen, M.A., A.P.G. van Heel and B.H.A.A. van den Brule, 1997, Simulation of viscoelastic flows using Brownian configuration fields, *J. Non-Newt. Fluid Mech.* **70**, 79-101.

Jendrejack, R.M., E.T. Dimalanta, D.C. Schwartz, M.D. Graham

and J.J. Pablo, 2003a, DNA dynamics in a microchannel, *Phys. Rev. Lett.* **91**, 038102.

Jendrejack, R.M., D.C. Schwartz, M.D. Graham and J.J. Pablo, 2003b, Effect of confinement on DNA dynamics in microfluidic devices, *J. Chem. Phys.* **119**, 1165-1173.

Lee, E.C., M.J. Solomon and S.J. Muller, 1997 , Molecular orientation and deformation of polymer solutions under shear, *Macromolecules* **30**, 7313-7321.

Öttinger, H.C., 1996, Stochastic processes in polymeric fluids, Springer, Berlin.

Öttinger, H.C., B.H.A.A. van den Brule and M.A. Hulsen, 1997, Brownian configuration fields and variance reduced CONNFFFESSIT, *J. Non-Newt. Fluid Mech.* **70**, 255-261.

Perkins, T.T., D.E. Smith and S. Chu, 1997, Single polymer dynamics in an elongational flow, *Science* **276**, 2016-2021.

Radzyner, Y. and D.C. Rapaport, 1998 , Orientational effects in the channel flow of flexible and rigid molecules, *Phys. Rev. E.* **57**, 5687-5693.

Schroeder, C.M., R.E. Teixeira, E.S.G. Shaqfeh and S. Chu, 2005, Dynamics of DNA in the flow-gradient plane of steady shear flow: Observations and simulation, *Macromolecules* **38**, 1967-1978.

Shrewsbury, P.J., S.J. Muller and D. Liepmann, 2001, Effect of flow on complex biological macromolecules in microfluidic devices, *Biomedical Microdevices*. **3**(3), 225-238.

Skjetne, P., R.F. Ross and D.J. Klingenberg, 1997, Simulation of single fiber dynamics, *J. Chem. Phys.* **107**, 2108-2121.

Smith, D.E., H.P. Babcock and S. Chu, 1999, Single-polymer dynamics in steady shear flow, *Science* **283**, 1724-1727.

Smith, D.E. and S. Chu, 1998, Response of flexible polymers to a sudden elongational flow, *Science* **281**, 1335-1340.

Somasi, M. and B. Khomami, 2000, Linear stability and dynamics of viscoelastic flows using time-dependent stochastic simulation techniques, *J. Non-Newt. Fluid Mech.* **93**, 339-362.

Teixeira, R.E., H.P. Babcock, E.S.G. Shaqfeh and S. Chu, 2005, Shear thinning and tumbling dynamics of single polymers in the flow-gradient plane, *Macromolecules* **38**, 581-592.

Usta, O.B., A.J.C. Ladd and J.E. Butler, 2005, Lattice-Boltzmann simulations of the dynamics of polymer solutions in periodic and confined geometries, *J. Chem. Phys.* **122**, 094902.

Woo, N.J., E.S.G. Shaqfeh and B. Khomami, 2004a, Effect of confinement on dynamics and rheology of dilute DNA solutions. I. Entropic spring force under confinement and a numerical algorithm, *J. Rheol.* **48**, 281-298.

Woo, N.J., E.S.G. Shaqfeh and B. Khomami, 2004b, Effect of confinement on dynamics and rheology of dilute DNA solutions. II. Effective rheology and single chain dynamics, *J. Rheol.* **48**, 299-318.